NOTES AND CORRESPONDENCE

Impact of Local Convective Cloud Systems on Summer Daytime Shelter Temperature

MOTI SEGAL

Department of Physics and Astronomy, University of Kansas, Lawrence, Kansas

GRAHAM FEINGOLD

CIRES, University of Colorado, Boulder, Colorado

16 December 1992 and 22 March 1993

ABSTRACT

The potential impact of daytime local summer convective cloud systems on shelter air temperature is illustrated by numerical modeling and observations. Prolonged reductions in surface solar irradiance due to cloudiness result in a noticeable decrease in shelter temperature over drylands and a moderate temperature fall over wet surfaces. When cloudiness is abruptly diminished, shelter temperature increases rapidly. Numerical modeling of downdrafts associated with rainfall in a dry convective atmosphere indicates a pronounced drop in shelter temperature (as high as 12°C). The modeling results are consistent with observations. The significance of the results and their potential applications are outlined.

1. Introduction

The impact of cloudy synoptic-scale systems, such as those associated with cyclones and fronts, on ground-level solar irradiance as well as on shelter temperature has been the subject of many studies. In these situations, solar irradiance and air temperature may be modified for several days (with a persistent reduction in solar radiation and temperature). Usually, shelter temperatures in these situations are reasonably forecasted. Also, the characteristics of the modification in the shelter temperature in these situations can be easily resolved, both spatially and temporally, from regular climatological data.

When short-lived convective cloud systems are considered, the relatively reduced spatial and temporal scales of the systems make it difficult to consider its impact on the air temperature (e.g., Maddox and Heckman 1982). These systems should be viewed as a local perturbation of weather prevailing in the region, where the large systems *determine the regional weather.* The present note evaluates the potential modification of shelter temperature associated with such short-lived convective cloud systems as a result of cloud shading as well as cooling from evaporation of rainfall. During summer these systems commonly occur as a result of daytime convection and are frequent in midlatitude regions in which the combined effects of moisture, a deep convective atmospheric boundary layer (ABL), and lifting mechanisms are pronounced. During fall and spring these systems are to some extent typical in subtropical latitudes and mostly in coastal areas. General climatological evaluations related to the cloudiness and precipitation of such systems are given by Wallace (1975), Klitch et al. (1985), and Weaver and Segal (1988).

In this note, modeling and observations provide *scaling* of the impact on shelter temperature of cloud shading and rain evaporation associated with local systems. The illustrations focus on the Front Range of Colorado. In section 2, numerical modeling estimations are given, whereas in section 3 evaluation based on observations is provided. Discussion and applied aspects of the various evaluations are given in section 4.

2. Numerical model evaluations

a. The effect of convective cloud shading on shelter air temperature

Although short-duration decreases in shelter air temperature due to cloud shading are common, no systematic modeling study attempts to relate their magnitude and duration to the characteristics of the decrease in near-surface solar irradiance. Some numerical model studies have involved selected illustrative evaluations (for example, Wetzel et al. 1984; Segal et al. 1986). In the present section, such previous studies are expanded through numerical model evaluations.

Corresponding author address: Moti Segal, Department of Physics and Astronomy, University of Kansas, Lawrence, KS 66405-2151.

1) THE MODEL

The model evaluations use the atmospheric numerical model described in detail by Mahrer and Pielke (1977). The atmospheric model accounts for ABL and surface-layer momentum, heat, and moisture transfer processes. It also considers heating–cooling effects associated with solar irradiance and longwave terrestrial radiation. A surface heat balance equation, accounting for the various surface thermal fluxes, is solved to obtain surface temperature. A soil module containing an equation for heat diffusivity, which considers the surface wetness, is also included. Validations of this model (e.g., Segal and Pielke 1981; Steyn and McKendry 1988, among others) indicate that the model reasonably resolves the meteorological shelter temperature.

The simulations reported in the present study use a one-dimensional version of the model. Thus, it is assumed that the area affected by cloud shading is sufficiently large and uniform so as to justify one-dimensional simulations. Simulations were carried out for various durations of shading and various reductions in the incoming solar irradiance at the surface (the initiation of the simulations is at 0600 MST). The related patterns of the air temperature at 2-m height above surface are presented for a summer case at latitude 39°N (mid-July conditions in Denver, Colorado). The input parameters used in the model simulations are the same as given in Table 1 of Segal et al. (1992). The simulations assume that the clouds have not yet reached precipitating stage and do not interfere dynamically with the atmospheric boundary layer. Three regimes of solar irradiance are considered: (i) clear sky; (ii) heavy cloud cover in which the solar irradiance reaching the surface is 0.2 of the clear-sky situation (given the surface albedo the absorbed solar irradiance is 0.16 of the clear-sky value), and (iii) moderate cloud cover with a corresponding solar irradiance reduction of 0.6 and absorbed solar irradiance of 0.48. The increase in longwave irradiance at the surface due to cloudiness was estimated according to the empirical relation given in Oke (1987), for example, with a resulting increase of 0.2 and 0.05 in both cases, respectively. The time-dependent simulated solar irradiance reaching the ground, E_G, for situations (i)–(iii) described above is presented in Fig. 1.

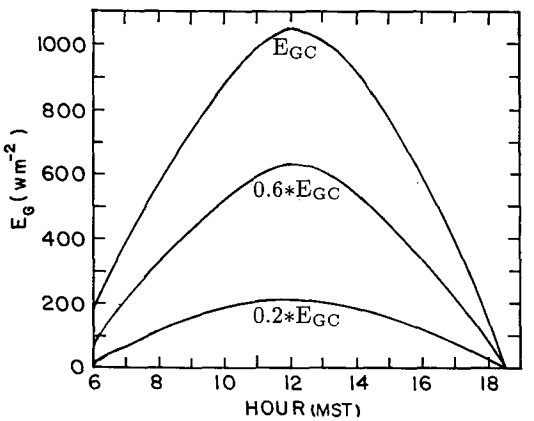

FIG. 1. Model-simulated diurnal solar irradiance E_G variation for the three sky conditions described in section 2a. (E_{GC}—clear sky, $0.6E_{GC}$—moderate cloud cover, $0.2E_{GC}$—heavy cloud cover.)

2) CASE A—HEAVY CLOUDINESS SHADING

A variety of scenarios of heavy cloud cover (when solar irradiance is 0.2 that of clear skies), inception and duration, and surface wetness were considered. Figures 2a,b present results obtained for a relatively dry surface, with a surface moisture availability of 0.05 (the surface moisture availability m expresses the ratio of evaporation to potential evaporation) and for various durations of cloud shading. The duration of the cloud shading is indicated by tick marks on the curves.

One hour after shading begins, the shelter temperature T_a drops 1°–2°C. Thereafter, for an extended shading period the pattern of temporal variation in T_a is similar to that of the clear-sky situation. Figure 2a presents situations of midday shading of various durations. The magnitude of the fall in T_a compared with the clear-sky reference depends on the duration of the shading: for a 1-h shading duration, the maximum temperature fall is approximately 2°C; for 7 h it reaches 6°C. Upon cessation of the cloud shading, however, a noticeable increase in the T_a values is simulated. These are followed by lower T_a values compared with the clear-sky simulation. For a continuous shading following its initiation, as anticipated, noticeable falls in T_a are indicated, as illustrated in Fig. 2b. When the shading is initiated late in the afternoon, a slight increase in T_a is simulated. This is attributed to the decrease in the net radiative cooling at the surface due to the increased incoming atmospheric longwave irradiance.

When similar scenarios to those presented in Figs. 2a,b were repeated except for a wet surface ($m = 0.5$), (Figs. 3a,b), similar patterns were obtained but with the following distinctions: (i) the temperature level was lower compared with the previous cases as a result of the suppressed sensible heat flux, and (ii) the decreases in temperature due to the shading were somewhat milder.

3) CASE B—MODERATE CLOUDINESS SHADING

Cases similar to those presented in Figs. 2a,b but with moderate cloudiness are shown in Figs. 4a,b (solar irradiance 0.6 of clear-sky value). As anticipated, the decreases in T_a are milder but in general resemble the previous patterns. Maximum temperature decreases of 3°C were simulated.

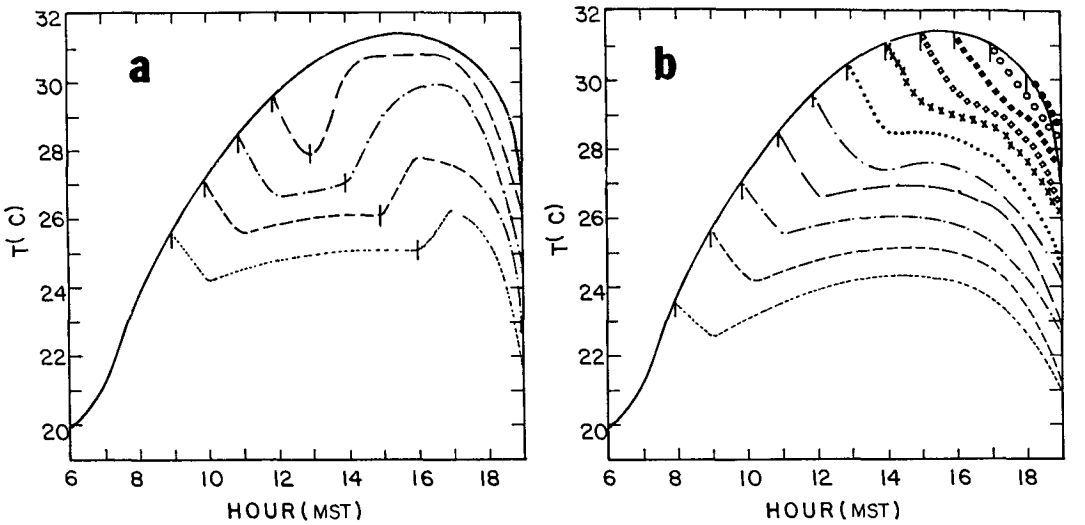

FIG. 2. Simulated diurnal variation of shelter temperature during summer in the Front Range of Colorado for a dry surface ($m = 0.05$). The solid curve presents the clear-sky situation. Clouds reducing the incoming solar irradiance at the surface to 0.2 were introduced for various periods: (a) for time period indicated by segment limited by two tick marks; (b) at various times of day as indicated by tick marks, and persisting for rest of day.

b. The effect of convective cloud precipitation on surface air temperature

Precipitation from convective clouds causes evaporative cooling, which results in downdrafts and a consequent drop in near-surface temperature. As the cool downdraft impinges on the ground, the divergent wind field can affect locations more than a few kilometers beyond the horizontal dimension of the rain shaft. However, the area affected by downdraft is typically much smaller than the area affected by shading. Model evaluations of evaporative cooling situations indicate that the potential drop in air temperature is sensitive to both macroscale properties such as the atmospheric background thermal and moisture characteristics, the dimensions of the rain shaft, and microphysical properties—that is, the size spectrum of the falling droplets (e.g., Srivastava 1985; Proctor 1988; Feingold et al. 1991). The following section offers a survey of relevant results from other works. In addition, selected numerical model simulations illustrate situations associated with isolated summer showers (typically of short duration) in the Front Range of Colorado.

1) PREVIOUS NUMERICAL SIMULATION RESULTS

(i) *Sensitivity to lapse rate of temperature*

One of the most important factors influencing the degree of cooling associated with precipitation is the lapse rate of temperature in the subcloud environment. Srivastava (1985), Proctor (1989), and Feingold et al. (1991) have shown how cooling increases as the lapse rate of temperature approaches the dry-adiabatic value

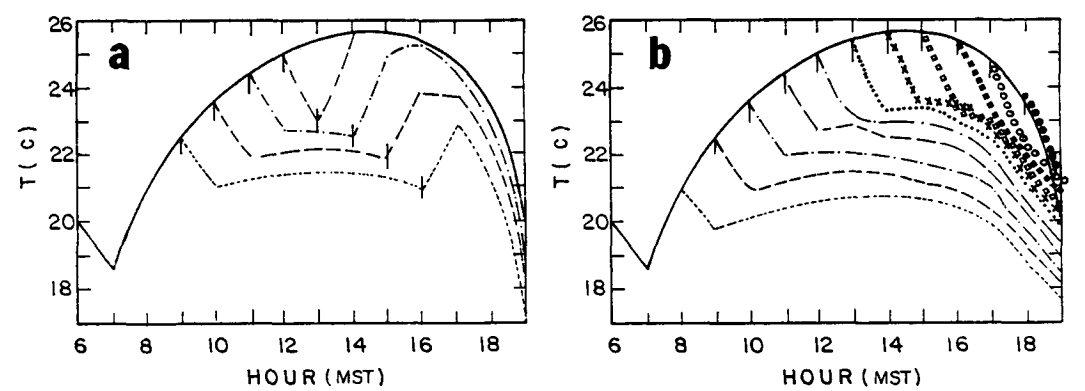

FIG. 3. Same as Fig. 2 except for wet surface conditions ($m = 0.5$).

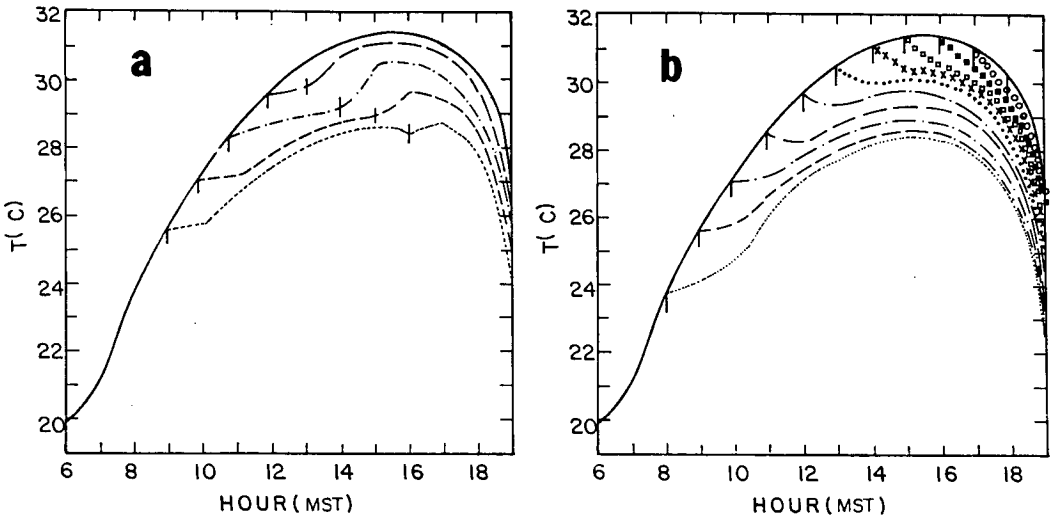

FIG. 4. Same as Fig. 2 except for cloud-reducing incoming solar irradiance at the surface to 0.6 of its clear-sky value.

of 9.8°C km^{-1}. In a one-dimensional model, Srivastava simulated near-ground cooling, ΔT_g, of the order of 2.5°C for a liquid water mixing ratio of 2.2 g kg^{-1} and a lapse rate of 9.5°C km^{-1}. These were probably underestimates of the cooling since one-dimensional models cannot simulate a downdraft impinging on the ground and thus tend to produce excessively vigorous downdrafts that have the relative effect of warming the air through compressional heating, which counteracts the cooling due to evaporation.

Proctor (1988, 1989) performed a number of numerical simulations of precipitation shafts using a 2D axisymmetrical model but without explicit treatment of the hydrometeor spectrum. Proctor (1989) used a variety of observed soundings with average lapse rates between 5.5°C km^{-1} and 9.4°C km^{-1}. For a 3-km-radius precipitation shaft and hydrometeor mixing ratio of 4.2 g kg^{-1} he simulated ΔT_g between 1.5° and 15°C, with the value increasing as the lapse rate approached the dry-adiabatic value.

Feingold et al. (1991) showed a ΔT_g of about 5°C for a dry-adiabatic lapse rate of temperature, liquid-water mixing ratio of 2.2 g kg^{-1}, and rain-shaft radius of 1 km. For identical conditions except for a lapse rate of 8°C km^{-1}, the value of ΔT_g was only 1°C.

(ii) *Sensitivity to hydrometeor mixing ratio*

For his baseline case (precipitation shaft radius of 3 km and hydrometeor mixing ratio of 4.2 g kg^{-1}), Proctor (1988) showed a ΔT_g of the order of 11°C after 15 min of precipitation. Note that because Proctor's hydrometeor spectrum at the top of the rain shaft was specified as hail a direct comparison with results for rain is not entirely correct. Nevertheless, as the latent heat of melting is only about one-eighth of that of evaporation, the differences are not great and are expected to be of the order of 10% (Proctor 1988). There will, however, be a difference in the vertical distribution of cooling, when ice, rather than water, is used as input to the model. Proctor (1989) performed a number of sensitivity studies on this baseline case for various hydrometeor mixing ratios. When a mixing ratio of 1.15 g kg^{-1} rather than 4.2 g kg^{-1} was used, the maximum ΔT_g was 7.5°C rather than 11°C. A hydrometeor mixing ratio of 0.3 g kg^{-1} produced weak cooling of only 2.2°C while a mixing ratio of 15.9 g kg^{-1} generated a maximum ΔT_g of 11°C, (i.e., of the same magnitude as for the baseline case of 4.2 g kg^{-1}). The extent of cooling becomes insensitive to the hydrometeor mixing ratio for values larger than about 4.2 g kg^{-1}.

(iii) *Sensitivity to the width of the precipitation shaft*

The degree of cooling is also strongly dependent on the width of the precipitation shaft. For rain shafts with radii of 0.25, 1.5, 3, and 5 km Proctor (1989) showed that the maximum cooling was 6°, 7.8°, 11°, and 12°C, respectively. Apparently the maximum cooling becomes insensitive to this parameter for precipitation shafts greater than about 3-km radius.

2) THE RAIN-SHAFT MODEL

A few simulations of rainfall typical of conditions in the Colorado Front Range were performed using the model of Feingold et al. (1991). Focus is placed on an evaluation of the effect on ΔT_g of the drop spectrum used as input at the top of the shaft. This two-dimensional axisymmetrical rain-shaft model solves prognostic equations for the vapor, temperature, water

mixing ratio, and wind fields. It also includes explicit treatment of the drop size spectrum. Because evaporation is a highly size-dependent process, it is important to treat all microphysical processes that affect the drop size distribution. Thus, the processes of evaporation and collision coalescence/breakup are solved using accurate moment-conserving methods. Details are furnished by Feingold et al. (1991). The current version of this model has been updated to include the force derived from the pressure perturbation in the equation for the vertical velocity w, as well as corrected drop evaporation rates as suggested by Srivastava and Coen (1992). A grid of 60 m in the vertical and 40 m in the radial direction is used.

3) Simulation results

To illustrate the effect of precipitation on the subcloud air temperature, we have simulated a case typical of conditions around Denver. The initial conditions consist of a dry-adiabatic layer from the ground up to cloud base at 3.2 km, a constant vapor mixing ratio profile, and a rain-shaft radius of 3 km. At the ground the air temperature is 32°C, the pressure is 850 mb, and the relative humidity is a rather low value of 20%. A drop spectrum with a liquid water mixing ratio of 4 g kg^{-1} and drop concentration of 0.01 cm^{-3} is prescribed at the top of the rain shaft for a period of 15 min. The drop size spectrum is assumed to be lognormal.

Figure 5a shows the vertical cross section of the cooling associated with the precipitation 15 min after initiation of the model. Maximum cooling is approximately 10°C, near the ground. Cooling is evident over a depth of about 1 km, well beyond the 3-km radius of the rain shaft. No precipitation reached the ground at radial distances greater than 3 km; thus, the cooling in this region is due to cold-air outflow or virga. Figure 5b shows values of ΔT_g as a function of radial distance from the center of the rain shaft. The results were obtained using the same initial conditions as in Fig. 5a, and differ only as regards the drop concentration of the rain. Thus, because the liquid water mixing ratio has been kept constant, an increase (decrease) in drop concentration is concomitant with a decrease (increase) in the average drop size. As shown in previous studies (Srivastava 1985; Feingold et al. 1991), evaporative cooling increases with a decrease in drop size (for the same liquid water mixing ratio). The reason for this is twofold: (i) the smaller drops present a greater surface area for evaporation, and (ii) the smaller drops fall more slowly than the larger drops and thus have more time to evaporate and cool the atmosphere.

In summary, these studies show that cooling increases with an increase in (i) lapse rate of temperature, (ii) the width of the rain shaft, (iii) mixing ratio of the hydrometeors, and (iv) drop concentration (for a fixed hydrometeor mixing ratio).

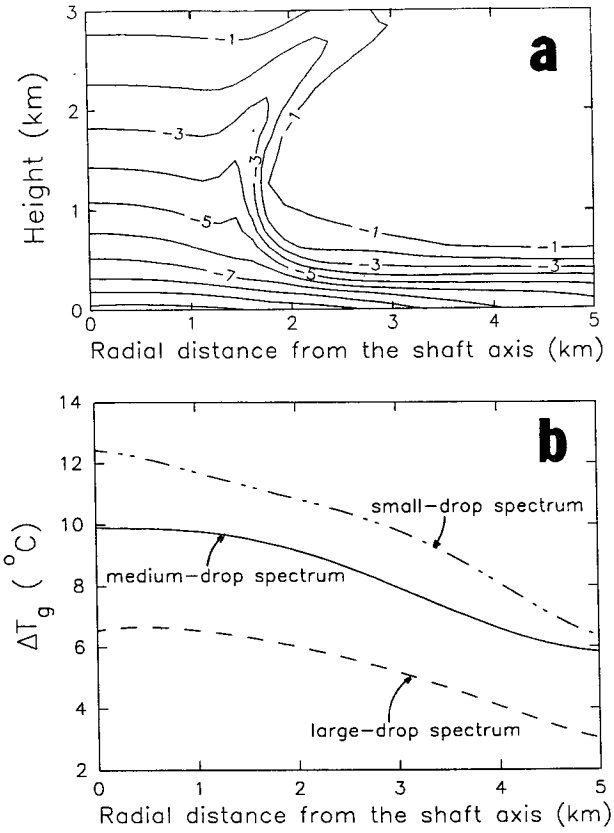

FIG. 5. (a) Vertical cross section of simulated fall in shelter temperature ΔT_a (°C) as a result of evaporative cooling associated with rainfall, for the drop spectrum, atmospheric background thermal stability, and specific moisture outlined in section 2b. (b) Simulated fall in shelter temperature near the ground ΔT_g as a result of evaporative cooling associated with rainfall characterized by three different size spectra. Background thermal stability and specific moisture are the same as in Fig. 5a.

For summertime conditions in the Front Range of Colorado, the modeling evaluations described in this section suggest cooling near the ground as high as about 12°C. Various simple, idealized situations can provide a means of scaling, or placing bounds on, the maximum temperature drop $\Delta T_{g\max}$.

(i) As a parcel of air descends from the shaft top along the moist-adiabatic curve (i.e., assuming that the shaft top is within the convective boundary layer and that the parcel acquires the wet-bulb temperature as evaporation brings it to saturation), the value of $\Delta T_{g\max}$ is given by

$$\Delta T_{g\max} = (\gamma_b - \gamma_m)h, \qquad (1)$$

where γ_m is the moist-adiabatic lapse rate, γ_b is the background lapse rate, and h is the height of the rain shaft. Thus, for h = 3 km, γ_b = 9.8°C km^{-1}, and the layer-averaged γ_m = 4.5°C km^{-1}, the maximum cooling near the surface is $\Delta T_{g\max}$ = 16°C. In reality, the lapse rate of the parcel does not achieve the moist-

adiabatic value since the drop spectrum contains fairly large drops with slow rates of evaporation. Therefore, lower values of $\Delta T_{g\max}$ are likely.

(ii) Another *bound* on $\Delta T_{g\max}$ can be obtained for drops falling and evaporating into a dry layer near the ground. Given sufficient time, this layer of air will achieve the wet-bulb temperature. For example, for the initial conditions used in these simulations (i.e., ground temperature 32°C, pressure 850 mb, and relative humidity at the ground about 20%), the wet-bulb temperature would be 16°C, representing a $\Delta T_{g\max}$ of 16°C. This value provides an upper bound on the cooling that can be achieved in this simple, idealized situation.

3. Observational evaluations

Real-time surface observations of total solar irradiance on a horizontal surface E_G, shelter temperature T_a, and rainfall amount P (all 5-min averages) were collected selectively during the summer of 1989 at various PROFS (Prototype Regional Operational Forecasting System) stations in the Front Range of Colorado (see Fig. 6 for site locations). In addition, GOES visible images of the area were obtained. These data present some illustration of the interrelation between shelter temperature and cloud shading and, occasionally, rainfall. Rainfall was determined from single surface measurements; some light rainfall events may not have been recorded, since the raingages have a resolution of only 0.25 mm. In these cases, there is some ambiguity in the interpretation of the observations; the absence of any recorded rainfall does not unequivocally imply that cooling was not associated with rain. As an illustration of this, the simulated rain discussed in section 2b produced just under 0.25 mm of rain during the first 200 s and would not have been recorded by the raingage. The near-ground cooling ΔT_g was at this stage about 4°C.

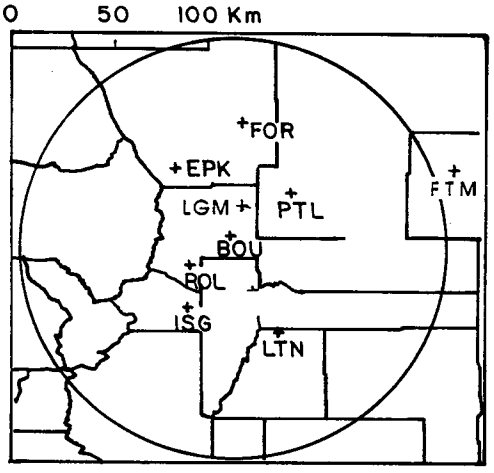

FIG. 6. Site locations of the PROFS mesonet stations used in study. BOU—Boulder, EPK—Estes Park, FOR—Fort Collins, FTM—Fort Morgan, LGM—Longmont, ISG—Idaho Springs, LTN—Littleton, PTL—Platteville, ROL—Rollinsville.

Horizontal thermal advection, which occasionally may have a significant effect on shelter temperature when cloud shading or rainfall conditions prevail, is not considered. Despite these limitations, preliminary insight into the patterns of T_a under these conditions can be gained.

The observations presented are of 2 June 1989, 28 June 1989, and 6 July 1989 (Fig. 7). GOES visible images of the Front Range of Colorado (Fig. 8) were available for the first three days and are presented in 30-min time intervals (for domain and location reference see Fig. 6). This information is useful in interpreting the patterns in Fig. 7. In Colorado, the daily maximum temperature is reached in summer around 1500 MST. Temporal changes in shelter temperature in the following illustrations are presented from around sunrise (0500 MST) until 1500 MST.

a. 2 June 1989

Generally a reduction in E_G is accompanied by a fall in temperature, most markedly when a sharp drop in E_G occurs (even for a relatively short period). In the latter case, even when rainfall at the stations is not recorded, either light rain (below raingage threshold), virga, or cold-air outflow from nearby areas affected by precipitation could be responsible for the drop in T_a.

In Fig. 7, a drop in T_a was recorded in BOU in association with a recorded rainfall event before 1500 MST. In LTN a sharp drop in E_G of about 2-h duration resulted in a noticeable fall in T_a. In ROL irregular variations in E_G were accompanied by noticeable changes in T_a. A pronounced fall in T_a ($\sim$5°C) around 1300 MST was concomitant with a sharp drop in E_G. This was followed, however, by an approximate 4°C warming as E_G reestablished itself to a normal level.

In FOR, a fluctuating E_G level resulted in T_a changes less than 1°C. However, toward the end of the period a reduction of E_G by 500 W m^{-2} during 1 h established a decreasing trend in T_a (this can be easily inferred by recalling that the daily maximum temperature occurs at about 1500 MST). A very sharp fall in E_G in LGM resulted eventually in an immediate temperature drop of approximately 3°C, suspected to be associated with light rain, virga, or cloud cold-air outflow.

b. 28 June 1989

In PTL, the afternoon hours show a reduced E_G associated with a decrease in T_a. Since the maximum T_a under clear sky conditions occurs around 1500 MST, it is projected that the 1500 MST was reduced by at

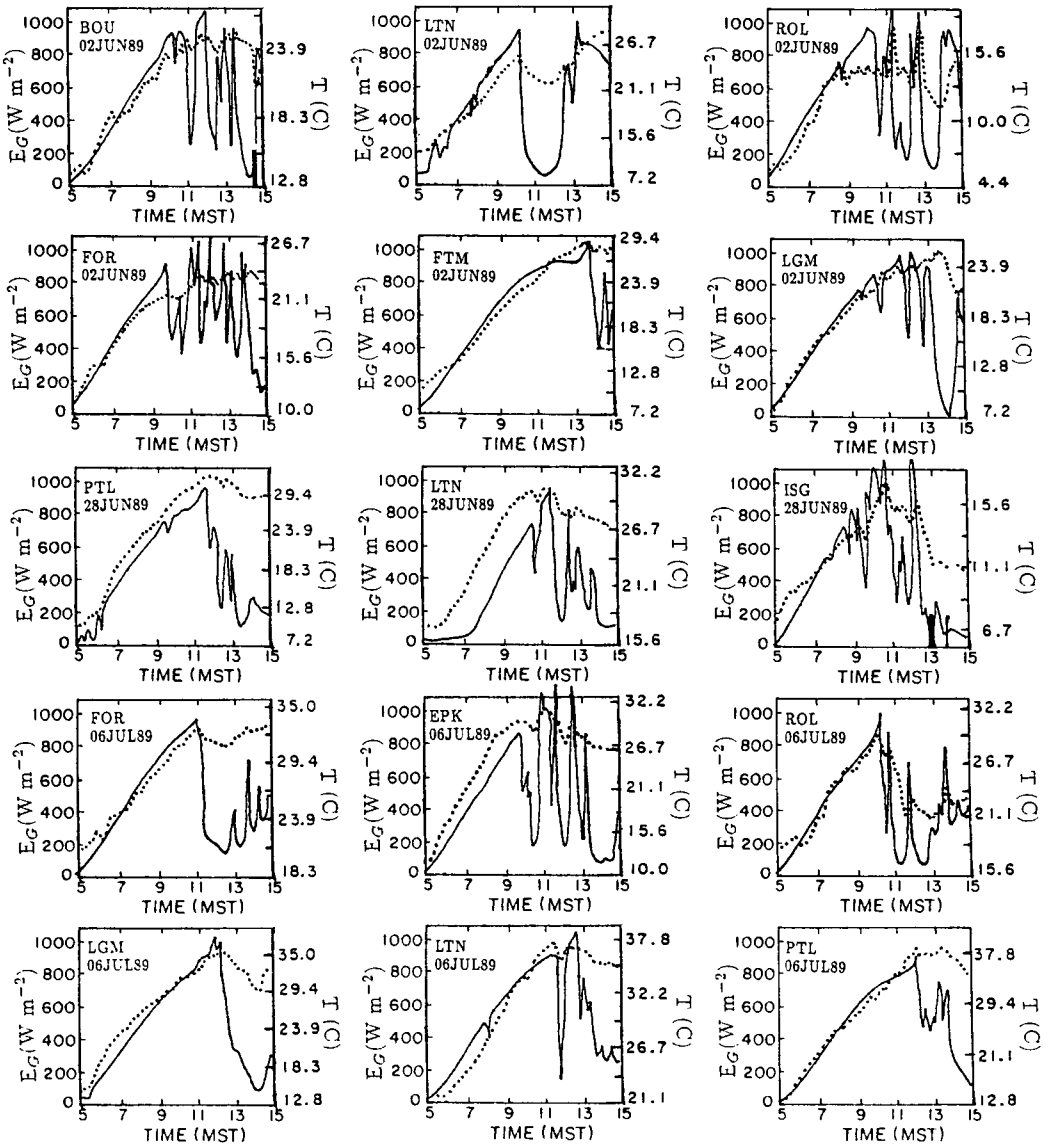

FIG. 7. Temporal changes in E_G (solid curves) and shelter temperature, T_a (dotted curves) while affected by cloud shading or rainfall. Rainfall amount P and duration are indicated by dark columns at BOU 2 June 1989, ISG 28 June 1989; during the indicated period the rainfall was 0.25 mm per 5 min.).

least 3°C. Such a reduction is even further emphasized in LTN. A sharper fall in T_a (>5°C), which was enhanced by rainfall, was observed in ISG during the afternoon.

c. 6 July 1989

A reduction of E_G in FOR during the afternoon led to a reduction in T_a estimated by 1500 MST to be about 3°C lower than the corresponding clear-sky situation. Reductions in E_G during the afternoon in EPK and in ROL were more noticeable. The 1130 MST sharp decrease in T_a recorded in ROL is probably associated with virga or cloud cold-air outflow (no rainfall was recorded at the ground, although small amounts of rain, below the raingage threshold of 0.25 mm, may have fallen). In LGM, LTN, and PTL the afternoon decrease in E_G is accompanied by a drop of up to approximately 4°C in T_a compared with the clear-sky situation.

d. Summary of the observations

The observations illustrate the interrelationships between E_G, T_a, and P.

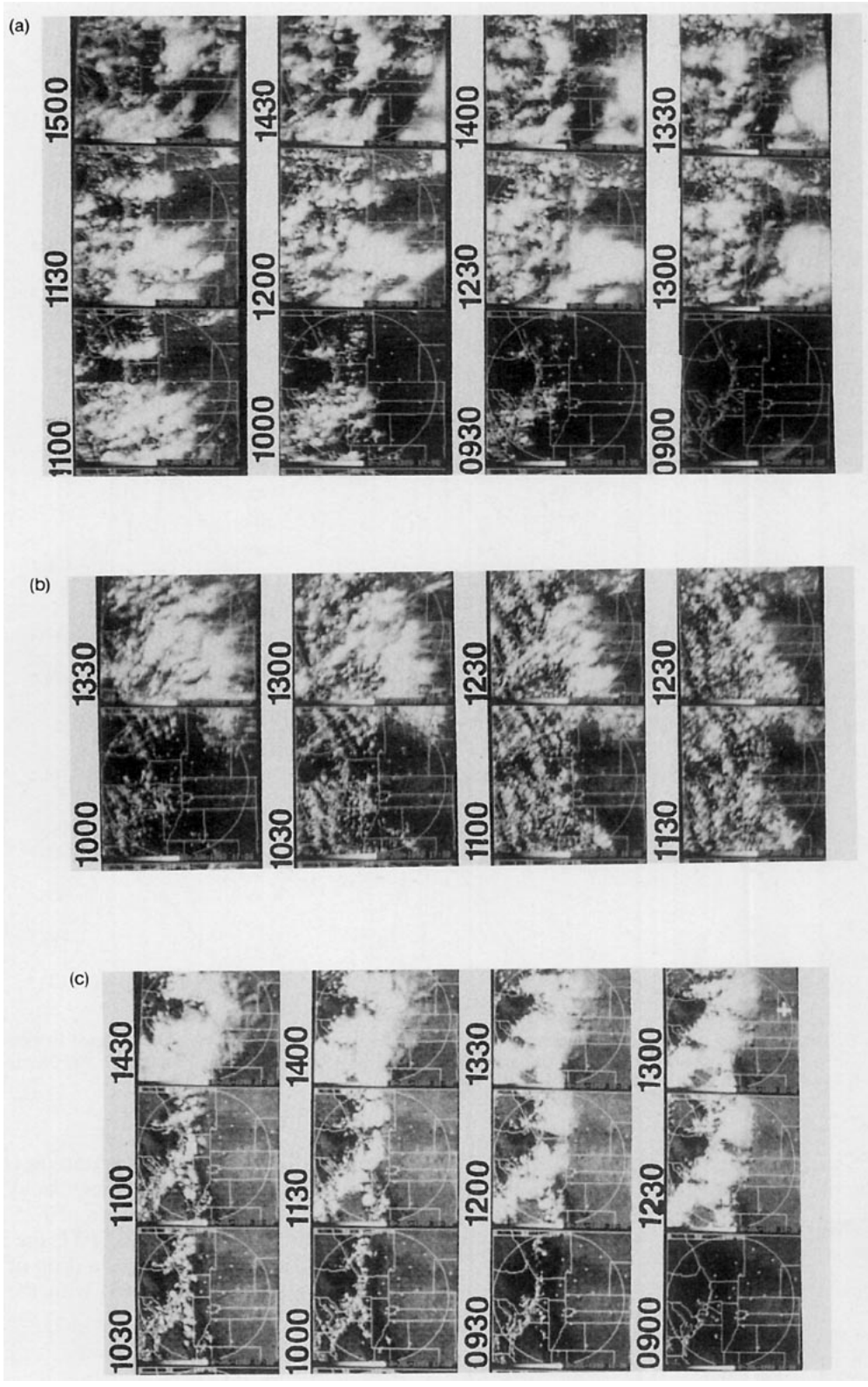

FIG. 8. GOES time sequence of visible images (in 30-min intervals) for (a) 2 June 1989 (first image at 0900 MST), (b) 28 June 1989 (first image at 1000 MST), and (c) 6 July 1989 (first image at 0900 MST).

(i) When precipitation was not recorded or implied, the quantitative interrelations between variations in E_G and T_a were in general agreement with the numerical model results in section 2.

(ii) When virga or cloud cold-air outflow were implied, the falls in T_a were typically as high as 5°C. (These events were assumed to be characterized by sharp, but short-duration, decreases in E_G, which were also associated with a sharp drop in T_a). For two of the presented shower events, the drops in T_a were somewhat higher.

Finally, in some of the E_G curves the effect of irradiance reflection by cloud walls is noted (see Segal and Davis 1992). These reflections occasionally support some increase in T_a.

4. Discussion

Assessment of the daily shelter temperature pattern as affected by synoptic-scale perturbations associated with overcast conditions is usually attained with reasonable success. The effects of cloud shading and of possible evaporative cooling due to precipitation, on the reduction of the shelter temperature, are embedded in such assessments. When summer local convective cloud systems are considered, the last two processes usually affect the temperature pattern for only a limited period, as evaluated in this note in an illustrative manner. The effect of cloud shading on the shelter temperature (which is dependent on the duration and amount of cloud cover as well as on the surface wetness) was evaluated by modeling and observations. Evaluations for summer conditions in the Front Range of Colorado showed that for prolonged daytime cloud shading, a decrease of several degrees Celsius in shelter temperature, compared with the clear-sky situation, is typical. However, when the cloud-shading duration is short and its reduction of solar irradiance is not extremely sharp, the impact on the temperature is considerably reduced. When a *sharp* drop in solar irradiance occurs in this region without recorded rainfall, there is some likelihood that air cooling is associated with either very light rainfall, virga, or cloud cold-air outflow.

Evaporative cooling associated with convective cloud precipitation usually has a noticeable impact on shelter temperature. The resulting rate of decrease in temperature is noticeably faster than that associated with cloud shading; however, the affected area is generally smaller than that associated with cloud shading. In this case the intensity of the temperature fall depends on the atmospheric background thermal stability, the specific humidity within the boundary layer, and the horizontal extent of the rainfall, as well as the rainfall rate and the size spectrum of rain drops. Model simulations for the Front Range of Colorado have indicated a potential drop in temperature as large as 12°C.

The impact of summer convective cloud shading and showers on temperature has importance in considerations of air conditioning, agriculture, and outdoor comfort. However, in urban areas most important, from an economic point of view, is the impact on air conditioning. A drop in air temperature (in addition to the related decrease in the solar irradiance) reduces the need for daytime air conditioning during summer. Understanding the pattern of the change in the temperature (while considering the change in solar irradiance or rainfall evaporation) may enable optimization of the air conditioning systems of large buildings. Also of importance are the operational aspects related to utility electric load management when a summer daytime decrease in temperature occurs over large urban areas. For example, Reiter (1985) reports a very high correlation between electric demand and air temperatures in Denver, Colorado, during the summer electric peak hours. Significant reduction in the electric load is common during sharp temperature drops. Taking into account the patterns presented in this note, together with forecasting/nowcasting of this situation based on satellite and radar measurements, may result in better efficiency in electric load management. It is suggested that the next step in studying the effects of convective cloud systems on shelter temperature should examine methodologies of quantification based on radar and satellite data.

Acknowledgments. The study was supported partially by NSF Grants ATM8616662 and ATM9114736. Some of the computations were carried out at the NCAR computer facility (NCAR is supported by the NSF). Observational data were provided by the PROFS-SERS at the Cooperative Institute for Research in the Atmosphere (CIRA) at CSU. Thanks are due to the Cloud Physics Group at the Tel Aviv University for performing calculations of the pressure perturbation term in the rainfall simulations. We would like to thank J. Brown, N. Doesken, J. Purdom, J. Weaver, and one of the reviewers for their comments. Thanks also to Reta Solwa for preparing the manuscript.

REFERENCES

Feingold, G., Z. Levin, and S. Tzivion, 1991: The evolution of raindrop spectra. Part III: Downdraft generation in an axisymmetrical rainshaft model. *J. Atmos. Sci.*, **48,** 315–330.

Klitch, M. A., J. F. Weaver, F. P. Kelly, and T. H. Vonder Haar, 1985: Convective cloud climatologies constructed from satellite imagery. *Mon. Wea. Rev.*, **113,** 306–337.

Maddox, R. A., and B. E. Heckman, 1982: The impact of mesoscale convective weather systems upon MOS temperature guidance. *Proc. 9th Conf. Weather Forecasting and Analysis,* Seattle, WA, Amer. Meteor. Soc., 214–218.

Mahrer, Y., and R. A. Pielke, 1977: The effects of topography on sea and land breezes in a two-dimensional numerical model. *Mon. Wea. Rev.*, **105,** 1151–1162.

Oke, T. R., 1987: *Boundary Layer Climates.* Methuen, 435 pp.

Proctor, F. H., 1988: Numerical simulations of isolated microburst. Part I: Dynamics and structure. *J. Atmos. Sci.*, **45,** 3137–3160.

——, 1989: Numerical simulations of isolated microburst. Part II: Sensitivity experiments. *J. Atmos. Sci.*, **46,** 2143–2165.

Reiter, E. R., 1985: Factors affecting energy use demand. *Handbook of Applied Meteorology,* D. D. Houghton, Ed., John Wiley and Sons, 846–889.

Segal, M., and R. A. Pielke, 1981: Numerical model simulations of human biometeorological heat load conditions—Summer day case study for the Chesapeake Bay area. *J. Appl. Meteor.*, **20,** 735–749.

——, and J. Davis, 1992: The impact of deep cumulus reflection on the ground-level global irradiance. *J. Appl. Meteor.*, **31,** 217–222.

——, G. Kallos, J. Brown, and M. Mandel, 1992: Morning temporal variations of shelter level specific humidity. *J. Appl. Meteor.*, **31,** 74–85.

——, J. F. W. Purdom, S. L. Song, R. A. Pielke, and Y. Mahrer, 1986: Evaluation of cloud shading effects on the generation and modification of mesoscale circulations. *Mon. Wea. Rev.*, **114,** 1201–1212.

Steyn, D. G., and I. G. McKendry, 1988: Quantitative evaluations of three dimensional mesoscale numerical model of sea breeze in complex terrain. *Mon. Wea. Rev.*, **116,** 1914–1926.

Srivastava, R. C., 1985: A simple model of evaporatively driven downdraft: Application to microburst downdraft. *J. Atmos. Sci.*, **42,** 1004–1023.

——, and J. L. Coen, 1992: New explicit equations for accurate calculation of the growth and evaporation of hydrometers by diffusion of water vapor. *J. Atmos. Sci.*, **49,** 1643–1651.

Wallace, J. M., 1975: Diurnal variations in precipitation and thunderstorm frequencies over the conterminous United States. *Mon. Wea. Rev.*, **103,** 406–419.

Weaver, J. F., and M. Segal, 1988: Some aspects of non-random cloudiness in solar energy application. *Solar Energy,* **41,** 49–54.

Wetzel, P., D. Atlas, and R. H. Woodward, 1984: Determining soil moisture geosynchronous satellite infrared data: A feasibility study. *J. Appl. Meteor.*, **23,** 375–391.